

NUMERICAL ANALYSIS OF RAYLEIGH-BÉRNARD CONVECTION USING LARGE EDDY SIMULATION AT HIGH RAYLEIGH NUMBERS

Shia-Hui Peng

Computational Physics, System Technology
Swedish Defence Research Agency (FOI)
SE-172 90 Stockholm, Sweden
peng@foi.se

Lars Davidson

Department of Applied Mechanics
Chalmers University of Technology
SE-412 96 Gothenburg, Sweden
lada@tfd.chalmers.se

Kemo Hanjalić

Department of Applied Physics
Delft University of Technology
2600 GA Delft, The Netherlands
hanjalic@ws.tn.tudelft.nl

ABSTRACT

Turbulent Rayleigh-Béarnard convection in a $6 : 1$ domain has been numerically studied using LES for Rayleigh numbers ranging from 6.3×10^5 to 10^9 . The results show reasonable agreement with previous experimental and DNS analysis. The scaling analysis with the present LES data shows that Nu may be scaled by a single relation of $Nu = 0.24Ra^{0.26}$, which lies approximately in line with the theoretical scaling for hard turbulence regime. In general, it was found that each characteristic scale considered can be fitted reasonably well with a single scaling relation. Nonetheless, for scales defined from thermal fluctuations and from properties in the off-wall mixed layer, to some extent, the transition from soft to hard turbulence has been reflected in the Ra -scaling between $Ra = 10^7$ and 4×10^7 . The transition is characterized by the thermal dynamics and, as Ra number increases, its occurrence seems to be more detectable in the mixed layer than near the wall.

INTRODUCTION

Rayleigh-Béarnard (RB) thermal convection has been extensively studied in a number of theoretical analysis, numerical modelling and experimental work, see e.g. Bodenschatz et al. (2000) for a recent review. The flow and thermal dynamics in RB convection depends on the geometrical setup, the temperature difference between the two horizontal boundaries and the fluid property, which have usually been cast into two dimensionless parameters, the Rayleigh number, $Ra = g\beta\Delta T_0 H^3 / (\nu\alpha)$, and the Prandtl number, $Pr = \nu/\alpha$, where $\Delta T_0 = (T_h - T_c)$ and H are respectively the temperature difference and the distance between the hot (T_h) and cold (T_c) horizontal surfaces, ν and α are, respectively, the molecular kinematic viscosity and thermal diffusivity of the fluid.

The scaling of the dynamic and thermal quantities with the Ra number is of particular interest. In previous experiments (Sano et al., 1989, Wu and Libchaber, 1992), it was found that the heat flux in terms of Nusselt number, Nu , obeys the classical $Ra^{1/3}$ scaling-law at lower Ra numbers. This scaling regime is termed *soft* turbulence. With increasing Ra number to $Ra = 4 \times 10^7$ and higher, the soft turbulence shifts to the so-

called *hard* turbulence regime following a $Ra^{2/7}$ scaling-law. Such features were numerically studied by Kerr (1996) using DNS with the Ra number up to $Ra = 2 \times 10^7$. It was shown that the scaling may follow a single regime of hard convective turbulence. Kenjeres and Hanjalić (1999) made transient RANS computations for Ra number up to 10^9 to examine the RANS method used in reproducing the coherent structure. For $Ra \leq 10^8$, Kimmel and Domaradzki (2000) examined their SGS estimation model in LES for the RB convection, where the heat transfer was over-estimated as compared with DNS and experimental data.

With Ra number up to 10^9 in the present study, LES has been performed for RB convection covering both the *soft* and *hard* convective turbulence regimes with a sufficient margin above the transitional Ra number. The main purpose of the work is to revisit some scaling relations in comparison with previous results. Effort has also been made in the scaling analysis of some dynamic and thermal properties in order to observe the Ra -dependence in response to the scaling regimes of soft and hard turbulence.

SIMULATION METHODOLOGY

The SGS model used in the simulation is the dynamic Smagorinsky model, where the model coefficient is determined using the dynamic procedure. A similar procedure is applied to the computation of the thermal field (Peng and Davidson, 1998), for which the gradient-diffusion hypothesis is employed to model the SGS heat fluxes.

The computations were carried out in a computational domain with rigid upper and lower boundaries at fixed temperature and periodic sidewalls. The aspect ratio of the numerical domain is $6 : 1 : 6$ and the Prandtl number is $Pr = 0.71$. Table 1 gives the mesh resolution at different Ra numbers. The dynamically determined SGS model coefficients are assumed to be functions of time and of only the inhomogeneous y -direction. A spatial averaging over the homogeneous x - and z -directions has been employed in the dynamic procedure to stabilize the numerical procedure. The statistic quantities (denoted by $\langle \cdot \rangle$) have been obtained being averaged with time and

Table 1: Grid resolution for different Rayleigh numbers.

Case	A	B	C	D	E
Ra	6.3×10^5	10^7	4×10^7	10^8	10^9
$N_x = N_z$	48	48	64	64	64
N_y	64	64	80	80	96

over the horizontal directions.

The grid-filtered governing equations are discretized on a collocated grid using the 2nd-order central differencing finite-volume method. The solution is advanced in time with the second-order Crank-Nicholson scheme. An implicit, fractional step method is used to solve the discretized equation system.

RESULTS AND DISCUSSION

A fluctuating quantity of the resolved field is denoted by $\phi' = \bar{\phi} - \langle \bar{\phi} \rangle$ and $\phi_{rms} = \langle \phi'^2 \rangle^{1/2}$. All the results presented below have been normalized using H , $u_0 = \alpha/H$ and ΔT_0 . A velocity component is thus scaled in terms of the Péclet number, $Pe = uH/\alpha$. At $Ra = 6.3 \times 10^5$ for vertical profiles, DNS data are available (Wörner, 1994), which have been included in the plotting where appropriate for comparison.

Figure 1 presents the distributions of the time-averaged SGS eddy viscosity, $\langle \nu_{sgs} \rangle$, across the fluid layer. With increasing Ra number, the SGS turbulence increases its intensity. For the highest Ra number ($Ra = 10^9$), $\langle \nu_{sgs} \rangle$ is less than 10 times of the molecular viscosity. This suggests that the grid resolution has, in general, enabled to retain a moderately low SGS effect on the resolved large structure.

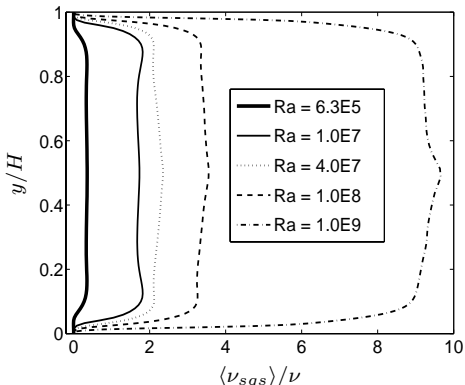


Figure 1: Time-averaged SGS viscosity, $\langle \nu_{sgs} \rangle / \nu$.

In Figure 2, the time-averaged resolved temperature, the r.m.s. temperature fluctuation and the resolved turbulent heat flux are presented, respectively. At $Ra = 6.3 \times 10^5$, the resolved temperature and heat flux agree well with the DNS data, whereas the thermal fluctuation is somewhat underestimated at the near-wall peak and across the center. The peak location of \bar{T}_{rms} , λ_T , agrees however with the DNS data. As Ra number increases, the centreline value of \bar{T}_{rms} , $\Theta_c/\Delta T_0$, reduces obviously, while the peak value, $\Theta_w/\Delta T_0$, is much less sensitive to increasing Ra number. For $Ra \geq 4 \times 10^7$, the distribution of $\langle v'T' \rangle$ in the center sinks due to the resolution, where the SGS contribution, $h_{\theta 2}$, becomes sensible. The characteristic height of the thermal boundary layer, λ_T , moves closer to the wall surface with increasing Ra number.

Figure 3 presents the vertical distribution of Nusselt num-

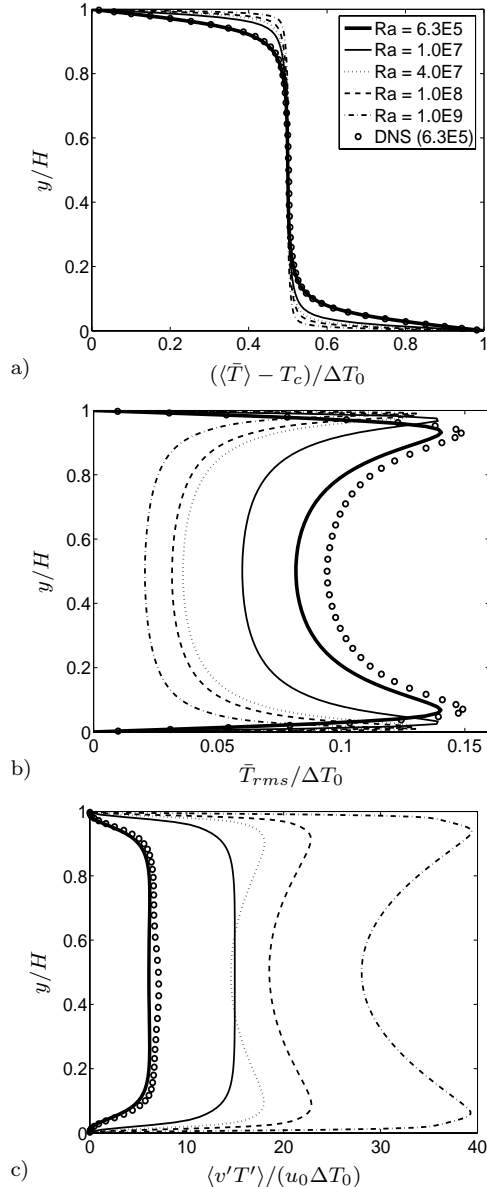


Figure 2: a) Time-averaged temperature, $(\langle \bar{T} \rangle - T_c)/\Delta T_0$. b) Resolved temperature fluctuation $\bar{T}_{rms}/\Delta T_0$. c) Resolved turbulent heat flux, $\langle v'T' \rangle / (u_0 \Delta T_0)$.

ber, $Nu(y)$, computed locally by

$$Nu(y) = \frac{\langle v'T' \rangle + \langle h_{\theta 2} \rangle - \langle \kappa \partial T / \partial y \rangle}{\kappa \Delta T_0 / H} \quad (1)$$

Note that the SGS heat flux, $\langle h_{\theta 2} \rangle$, has also been taken into account. $Nu(y)$ has an uniform distribution across the box, which suggests that the time used for averaging is sufficient to get the mean value of heat transfer.

In Figure 4 a), the vertical velocity fluctuation, \bar{v}_{rms} , is presented. Note that the two horizontal velocity components, \bar{u}_{rms} and \bar{w}_{rms} , have the same distribution due to the horizontal flow homogeneity. They are combined into a horizontal velocity fluctuation, $u_{hrms} = (\bar{u}_{rms}^2 + \bar{w}_{rms}^2)^{1/2}$, of which the distribution is shown in Figure 4 b). The total resolved turbulence kinetic energy, $K = (u_{hrms}^2 + \bar{v}_{rms}^2)/2$, is also plotted in Figure 4 c). The LES data show promising agreement

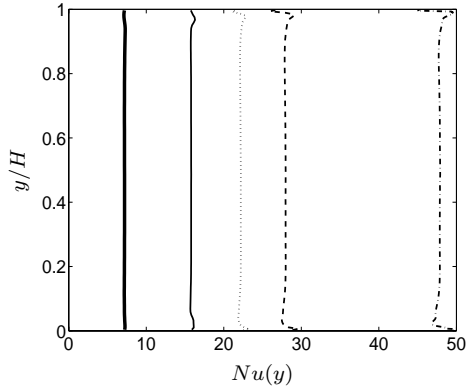


Figure 3: Time-averaged normalized heat flux, $Nu(y)$.

with DNS data at $Ra = 6.3 \times 10^5$. With increasing Ra number, unlike the temperature fluctuation being weakened, the velocity fluctuation increases. This is because the updraft and downdraft have *impinged* on the horizontal walls and entailing intensified horizontal motions. It is shown that the distribution of horizontal velocity fluctuation, u_{hrms} , is fairly flat across the center of the box, but exhibiting a near-wall peak, indicating the presence of near-wall shear. On the other hand, \bar{v}_{rms} increases all the way from the wall to the center, which has been caused due to the convective updrafts and downdrafts in the vertical direction, arising from the hot lower wall and descending from the cold upper wall respectively. The distribution of the total resolved kinetic energy, K , presents a broad and enlarged plateau over the central mixed layer with increasing Ra number and, consequently, the diffusive wall-layer being narrowed.

In the scaling analysis below, the centreline and near-wall peak values of u_{hrms} , as well as the centreline value of \bar{v}_{rms} , denoted respectively by u_{hc} , u_{hw} and v_c , will be used to define three characteristic velocity scales. Moreover, a length scale, λ_u , is measured at the peak location of u_{hrms} to characterize the velocity boundary-layer height.

Figure 5 a) plots the skewness of the vertical velocity, $S_v = \langle v'^3 \rangle / (\langle v'^2 \rangle)^{3/2}$, which indicates the degree of asymmetry of the convective downdrafts and updrafts. Positive skewness implies that the vertical convection is characterized by large areas of weak downdrafts and small areas of strong updrafts, while negative skewness suggests that intense downdrafts with small areas surrounded by large areas of weak updrafts. As Ra number increases, the region with large skewness becomes thin and, across the center of the box, the skewness profile approaching to a zero slope.

Along with S_v , the third central moment of vertical velocity, $\mu_3 = \langle v'^3 \rangle$, is worth being observed. The distribution of $sign(\mu_3)|\mu_3|^{1/3}/u_0$ is given in 5 b), showing that $|\mu_3|_{max}/u_0^3$ increases with increasing Ra number. μ_3 indicates the intensity of the descending/ascending drafts penetrating toward the opposite wall, characterizing the vertical turbulent transport of kinetic energy throughout the fluid layer. Kerr (1996) has argued that the incoming plumes and negative S_v may be an important ingredient in producing the shear that are used to explain hard turbulence scaling. In this work, the normalized cubic root of $|\mu_3|_{max}$, namely, $u_{v3}/u_0 = |\langle v'^3 \rangle|_{max}^{1/3}/u_0$, is taken to define a velocity scale. The corresponding peak-location of μ_3 , λ_{v3} , is also adopted for length-scale scaling.

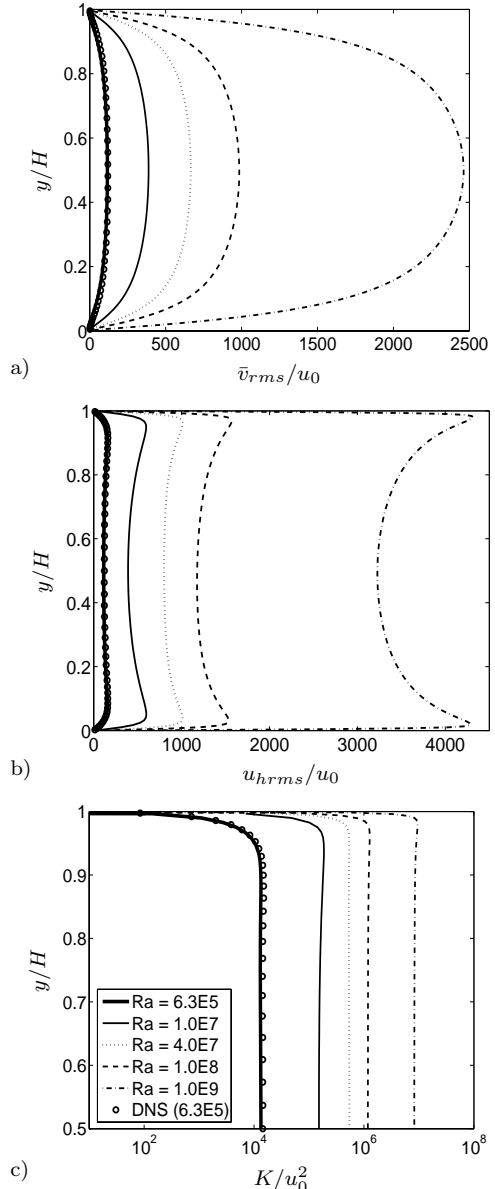


Figure 4: a) Vertical velocity fluctuation, \bar{v}_{rms}/u_0 . b) Horizontal velocity fluctuation, u_{hrms}/u_0 . c) Resolved total turbulence kinetic energy, K/u_0^2 .

In order to observe the intensity of shear, Figure 6 plots the magnitude of flow strain rate, $|\bar{S}| = \sqrt{2\bar{S}_{ij}\bar{S}_{ij}}$, where $\bar{S}_{ij} = (\partial\bar{u}_i/\partial x_j + \partial\bar{u}_j/\partial x_i)/2$. It is shown that across a large central portion of the box, $|\bar{S}|$ is relatively small and has a uniform distribution, yet its value on the wall, S_w , is rather large, implying significant wall shear. The centreline and wall values of $|\bar{S}|$, S_c and S_w , are taken in the scaling analysis to investigate the Ra -dependence of these quantities. Note that S_c and S_w have a reciprocal dimension of time scale. The sharp change of $|\bar{S}|$ from S_w to S_c near the wall indicates shear in the vicinity of the wall (the diffusive layer). By means of the $|\bar{S}|$ -distribution, we define a new length scale to characterize the height of the near-wall shearing layer, viz.

$$\lambda_s = \frac{\int_0^H |\bar{S}| dy - S_c H}{S_w - S_c} \quad (2)$$

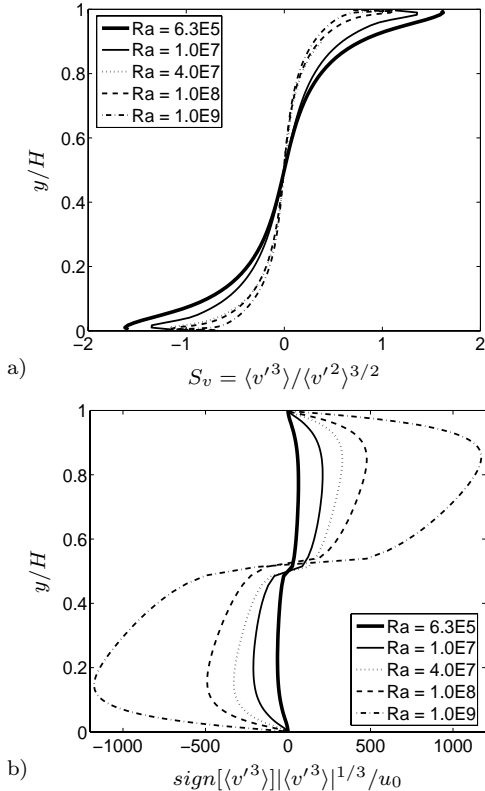


Figure 5: a) Skewness of vertical velocity. b) Cubic root of the third central moment of vertical velocity.

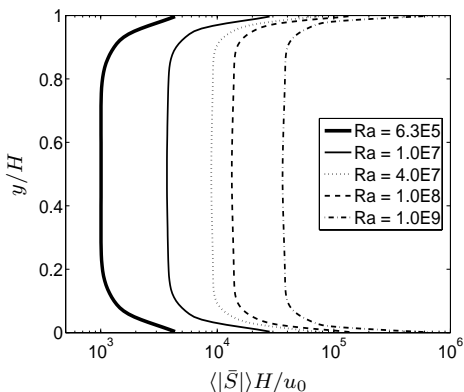


Figure 6: Time-averaged magnitude of resolved flow strain rate.

With the scales defined on the basis of the vertical profiles as addressed above, a Ra -scaling analysis is carried out in the range of $Ra \in [6.3 \times 10^5, 10^9]$, which covers the transition regime (at $Ra_{tr} \approx 4 \times 10^7$) from soft turbulence to hard turbulence, as observed in previous experimental analysis. In the DNS for $Ra \leq 2 \times 10^7$ by Kerr (1996), it was found that a single scaling regime corresponding to the hard convective turbulence can be established to represent the Ra -dependence, being applicable for the heat transfer and several velocity and temperature scales. Note that the 6 : 1 domain used in the present LES is the same as in the DNS by Kerr (1996).

The main purpose with the present Ra -dependence analysis is twofolds: investigating the scaling relations covering the soft and hard turbulence regimes based on the present LES

Table 2: Ra -scaling of flow and thermal quantities, $\sim CRa^\beta$. (Note that the superscript * denotes the normalization by u_0 , H and ΔT_0).

	u_{hw}^*	u_{hc}^*	v_c^*	Θ_w^*	Θ_c^*
C	0.411	0.262	0.479	0.166	1.166
β	0.447	0.458	0.413	-0.0125	-0.194
	S_w^*	S_c^*	u_{v3}^*	$u_{\tau w}^*$	Nu
C	0.484	1.393	0.348	0.649	0.243
β	0.687	0.494	0.393	0.340	0.257

Table 3: Ra -scaling of the length scales, $\sim CRa^\beta$

	λ_u/H	λ_T/H	λ_s/H	λ_{v3}/H
C	1.335	2.395	0.940	0.510
β	-0.204	-0.269	-0.186	-0.0625

computations, and making comparison with the experimental and DNS-derived scaling laws. Based on the present LES data and assuming a single scaling relation for each characteristic scale, the Ra -dependence of these scales is summarized in Tables 2 and 3.

Figure 7 plots the Nusselt number, Nu , versus Ra number. Note that the Nusselt number can be calculated at the wall by $Nu_w = -H\langle\partial T/\partial y\rangle_w/\Delta T_0$. Both the integrated $Nu(y)$ (from Eq. (1)) and Nu_w have been included in Figure 7, showing a negligible difference. The scaling does not exhibit obvious transition at $Ra_{tr} = 4 \times 10^7$, for which theoretical analysis indicates that 1/3- and 2/7-scaling laws are applicable for soft and hard convective turbulence, respectively. The LES data agrees reasonably well with the scaling relations generated from previous experiment and DNS data. A least squares fit of the present LES data gives $Nu = 0.243Ra^{0.257}$.

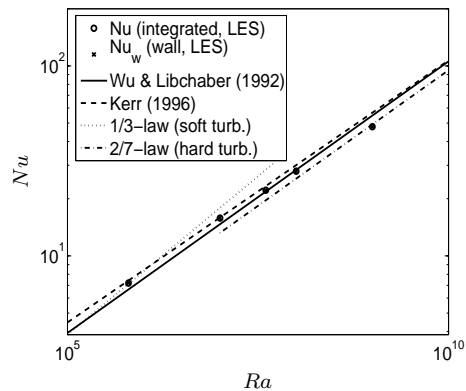


Figure 7: Nusselt number versus Rayleigh number. Also plotted are the experiment Ra -scaling $0.146Ra^{0.286}$ (Wu and Libchaber (1992) and DNS Ra -scaling $0.186Ra^{0.276}$ (Kerr, 1996).

The normalized temperature scales for $\Theta_w = \bar{T}_{rms,max}$ and $\Theta_c = \bar{T}_{rms,center}$ are plotted in Figure 8. Also plotted in this figure are the scaling relations derived from DNS data by Kerr (1996), where $\Theta_c/\Delta T_0$ and $\Theta_w/\Delta T_0$ were forced to fit with the $Ra^{-1/7}$ and $Ra^{-1/14}$ laws, respectively. As shown, the LES data is in large discrepancy from these scaling relations that have been regressed with the DNS data for $Ra \leq 2 \times 10^7$ (Kerr, 1996). Similar to the DNS data, with increasing Ra number, LES reproduces the temperature fluctuation much

less steep near the wall than in the center. Both temperature scales present a somewhat sharp drop from $Ra = 10^7$ to 4×10^7 , where the transition from soft to hard turbulence is supposed to occur. With the theoretical scaling laws, $\Theta_c/\Delta T_0 \sim Ra^{-1/9}$ and $Ra^{-1/7}$ for soft and hard turbulence, respectively, $\Theta_c/\Delta T_0$ shows a fairly good agreement. The Ra -dependence of $\Theta_w/\Delta T_0$ is rather weak. From $Ra = 10^7$ to 4×10^7 , $\Theta_w/\Delta T_0$ reduces by about 10%. For smaller and larger Ra numbers, $\Theta_w/\Delta T_0$ exhibits an insensible dependence on Ra number. This is reflected in the least squares fit with a less-slope scaling relation of $\Theta_w/\Delta T_0 = 0.166Ra^{-0.0125}$. The present LES gives $\Theta_c/\Delta T_0 = 1.166Ra^{-0.194}$, which gives a nearly parallel Ra -scaling relation to the experimental result, $\Theta_c/\Delta T_0 = 1.9Ra^{-0.20}$, by Wu and Libchaber (1992), though the LES values of $\Theta_c/\Delta T_0$ are somewhat underestimated.

The Ra -scaling for $\Theta_w/\Delta T_0$ and $\Theta_c/\Delta T_0$ indicates that these thermal scales are sensitive to the transition from soft to hard turbulence regime between $Ra = 10^7$ and 4×10^7 .

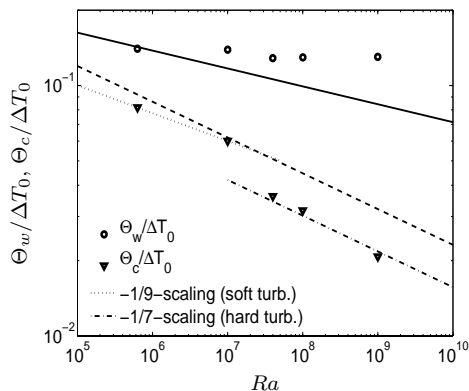


Figure 8: Ra -dependence of \bar{T}_{rms} in the center and at the near-wall peak, $\Theta_c/\Delta T_0$ and $\Theta_w/\Delta T_0$. Solid line indicates DNS Ra -scaling (Kerr, 1996) for $\Theta_w/\Delta T_0 = 0.37Ra^{-1/14}$, and dashed line for $\Theta_c/\Delta T_0 = 0.62Ra^{-1/7}$.

In Figure 9, several velocity scales are plotted versus Ra number. A wall-friction velocity scale defined by $u_{\tau w} = \sqrt{\nu \partial u_{hrms} / \partial y|_{wall}}$ is also included to observe the Ra -dependence of wall shear. Unlike in DNS, the LES data for u_{hw}/u_0 and v_c/u_0 do not hold the same Ra scaling. It was found that u_{hw}/u_0 agrees closely with the 4/9-scaling for soft turbulence, having $u_{hw}/u_0 = 0.411Ra^{0.447}$. The scaling relation, $v_c/u_0 = 0.479Ra^{0.413}$, fits reasonably well with the 3/7-law for hard turbulence. The wall-friction velocity, $u_{\tau w}/u_0 \sim Ra^{0.34}$ follows approximately the $Ra^{1/3}$ scaling, which is the theoretical scaling-law for Nu in the soft turbulence regime. Except for v_c/u_0 , which shows slight regressions with the scaling relations respectively in the soft and hard turbulence regimes, there is no obvious transition observed for other velocity scales.

The two characteristic boundary-layer heights, λ_u and λ_T , are plotted in Figure 10. As with DNS, LES shows that $\lambda_u > \lambda_T$, but estimates a smaller difference than scaled by the DNS data between the two boundary-layer heights at the same Ra number. The soft-to-hard turbulence transition is not sensibly reflected in the scaling for λ_u , but slightly for λ_T . A single scaling relation for each is applicable. The scaling for the thermal boundary-layer height, $\lambda_T/H = 2.395Ra^{-0.269}$, agrees reasonably well with the theoretical scaling of $Ra^{-2/7}$ in the hard turbulence regime.

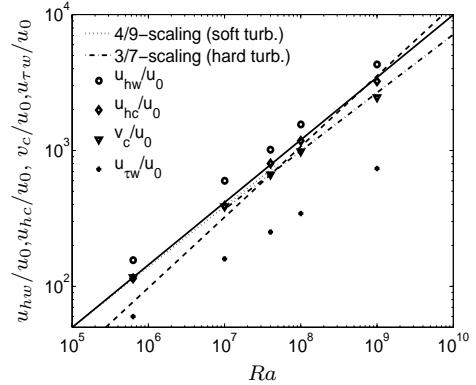


Figure 9: Ra -dependence of near-wall peak value of u_{hrms} , u_{hw}/u_0 , the centreline values of u_{hrms} and v_{rms} , u_{hc}/u_0 and v_c/u_0 , and a wall-friction velocity, $u_{\tau w}/u_0$. Solid line indicates DNS Ra -scaling (Kerr, 1996) for u_{hw}/u_0 and v_c/u_0 with $0.25Ra^{0.46}$, and dashed line for $u_{hc}/u_0 = 0.074Ra^{0.52}$.

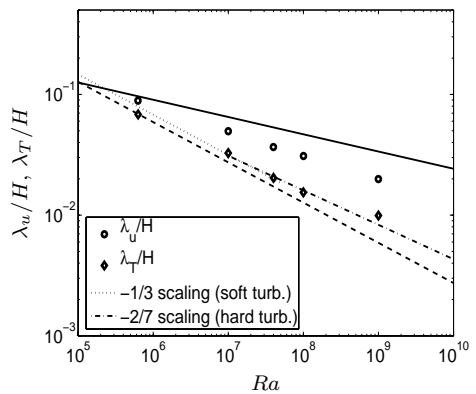


Figure 10: Ra -dependence of λ_u/H and λ_T/H . Solid line indicates DNS Ra -scaling (Kerr, 1996) for $\lambda_u/H = 0.65Ra^{-1/7}$, and dashed line for $\lambda_T/H = 5.9Ra^{-1/3}$.

Figure 11 a) presents the Ra -dependence of the normalized velocity scale defined from $\langle v'^3 \rangle$, i.e. $u_{v3}^* = |\langle v'^3 \rangle_{max}|^{1/3}/u_0$, where the wall (S_w) and centreline (S_c) values of $|\bar{S}|$ are also plotted. It is shown that each quantity may be fitted best with a single scaling relation, but S_c^* exhibits a very slight jump at $Ra = 4 \times 10^7$. In addition, it should be noted that the scaling of $u_{v3}^* \sim Ra^{\beta_{u\tau}}$ can be related to the scaling of $S_w^* \sim Ra^{\beta_{S_w}}$ with $\beta_{S_w} \approx 2\beta_{u\tau}$, as shown in Table 2.

The scaling for λ_s and λ_{v3} , defined respectively by Eq. (2) and from the location of the maximum value of $\langle v'^3 \rangle$, is shown in Figure 11 b). Note that λ_s is a characteristic height for the near-wall shearing layer, which is comparable with λ_u , but decreasing relatively slowly with increasing Ra number. In general, λ_{v3} is measured out of the near-wall diffusive layer. As shown in 11 b), λ_{v3} shows a fairly slight Ra -dependence. For Ra numbers less than 4×10^7 , λ_{v3}/H reduces relatively quickly as Ra number increases. Above $Ra = 4 \times 10^7$, λ_{v3}/H exhibits only a weak Ra -dependence.

The scaling property over the soft and hard turbulence regimes seems to be more sensitive to the Ra number in the off-wall mixed layer. In Figure 12, the centreline values for the resolved total kinetic energy, K , and the SGS viscosity, $\langle \nu_{sgs} \rangle$, are plotted, which represent, respectively, the turbulence intensities for the resolved large-scale and modeled small-scale structures. The scaling of $\sqrt{K_c}/u_0 = 0.40Ra^{3/7}$ complies with

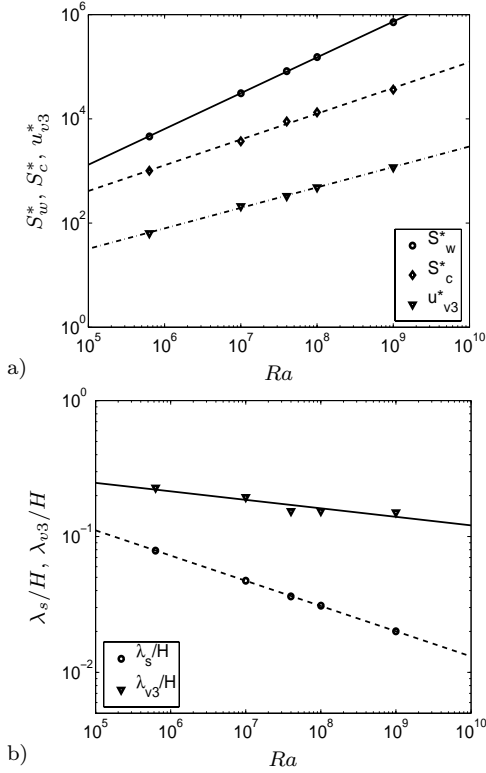


Figure 11: (a) Ra -dependence of $|\bar{S}|$ on the wall and in the center, $S_w^* = S_w H/u_0$ and $S_c^* = S_c H/u_0$, and of the maximum value of $u_{v3}^* = |\langle v'^3 \rangle|_{max}^{1/3}/u_0$; (b) Ra -dependence of λ_s/H and λ_{v3}/H . The lines are the least squares fits, given in Tables 2 and 3.

the velocity scaling relation in the hard turbulence regime. The $\langle \nu_{sgs} \rangle_c$ -scaling displays a somewhat different slope from $Ra = 10^7$ to 4×10^7 . This may imply a transition from soft to hard turbulence regime, in which a role has been played by the dynamics of small-scale turbulence.

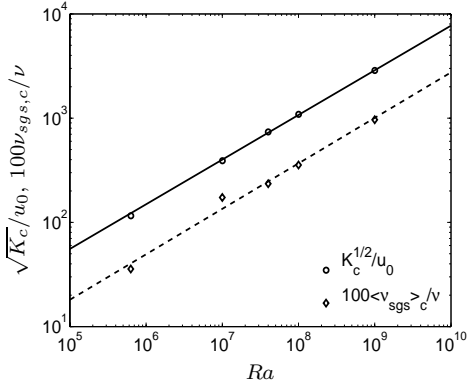


Figure 12: Ra -dependence of the centreline values for K and $\langle \nu_{sgs} \rangle$. The least squares fits are respectively $\sqrt{K_c}/u_0 = 0.4Ra^{3/7}$ and $\langle \nu_{sgs} \rangle_c/\nu = 0.0012Ra^{0.44}$.

CONCLUSIONS

RB convection has been computed using LES for $Ra \in [6.3 \times 10^5, 10^9]$, covering the transition regime from soft to hard turbulence. The result demonstrates reasonable agreement with available DNS data at $Ra = 6.3 \times 10^5$. It is shown that, with increasing Ra number, the normalized velocity fluctua-

tion is generally intensified, whereas the thermal fluctuation is obviously alleviated apart from the thin, near-wall layer. The near-wall peak of the horizontal velocity fluctuation indicates the presence of shear.

The main focus of this work is on the Ra -scaling analysis, for which a number of scales have been revisited in comparison with existing experimental and DNS results. The study has confirmed previous DNS analysis for the heat transfer, namely, the scaling of Nu can be established with a single relation that is approximately consistent with the scaling law in the hard turbulence regime, which holds also to some extent for the thermal boundary layer height, λ_T/H , and for the velocity scales defined from the horizontal velocity fluctuation. In general, it was found, over the soft and hard turbulence regimes, a single scaling relation is reasonably applicable for each characteristic scale considered.

Nonetheless, there exist several quantities, of which the scaling shows a sensible response to the transition between $Ra = 10^7$ and 4×10^7 . Such quantities include $\Theta_w/\Delta T_0$, $\Theta_c/\Delta T_0$ and the length scale λ_{v3}/H . Additionally, v_c/u_0 and S_c^* respond also to the transition, being rather weak though. In view of these observations and that these quantities have been either derived from thermal fluctuations or defined in the off-wall region, it seems plausible to argue that the occurrence of transition in the Ra -scaling is more detectable in the off-wall mixed layer and by the thermal properties in relation to updrafts and downdrafts. Finally, it is remarked here that we realize that the resolution at higher Ra numbers may not be sufficient in the present LES, as being reflected in the predicted heat transfer. Nevertheless, the LES results are shown in line with the generally accepted trends in the Ra -scaling.

REFERENCES

- E. Bodenschatz, W. Pesch, and G. Ahlers. Recent development in Rayleigh-Bénard convection. *Annual Review of Fluid Mechanics*, 32:709–778, 2000.
- B. Castaing, G. Gunaratne, F. Heslot, L. Kadanoff, A. Libchaber, S. Thomae, X. Wu, Z. Zaleski, and G. Zanetti. Scaling of hard thermal turbulence in Rayleigh-Bénard convection. *J. Fluid Mech.*, 204:1–30, 1989.
- K. Kenjeres and K. Hanjalic. Transient Analysis of Rayleigh-Bénard Convection with a RANS model. *Int. J. Heat and Fluid Flow*, 20:329–340, 1999.
- M. R. Kerr. Rayleigh number scaling in numerical convection. *J. Fluid Mech.*, 310:139–179, 1996.
- S. J. Kimmel and J. A. Domaradzki. Large eddy simulations of Rayleigh-Bénard convection using subgrid scale estimation model. *Physics of Fluids*, 12:169–184, 2000.
- S.-H. Peng and L. Davidson. Comparison of subgrid-scale models in LES for turbulent convection flow with heat transfer. In *Turbulent Heat Transfer 2*, pages 5.24–5.35, Manchester, UK, 1998.
- M. Sano, X. Z. Wu, and A. Libchaber. Turbulence in helium-gas free convection. *Phys. Rev. A*, 40:6421–6430, 1989.
- M. Wörner. Direkte simulation turbulenter Rayleigh-Bénard konvektion in flüssigem natrium. Dissertation University of Karlsruhe, KfK 5228, Kernforschungszentrum Karlsruhe, 1994.
- X. Z. Wu and A. Libchaber. Scaling relation in thermal turbulence: The aspect-ratio dependence. *Phys. Rev. A*, 45: 842–845, 1992.